# Numerical Simulation on the Formation of Mesoscale Vortex in Col Field

JIANG Yongqiang[1,2] (姜勇强) and WANG Yuan[1*](王 元)

1 *Key Laboratory of Mesoscale Severe Weather/Ministry of Education of China, and School of Atmospheric Sciences, Nanjing University, Nanjing* 210093

2 *Institute of Meteorology, PLA University of Science and Technology, Nanjing* 211101

(Received February 28, 2011; in final form September 15, 2011)

**ABSTRACT**

There exist typically two kinds of low-level col fields over the middle and lower reaches of the Yangtze River of China during summer. One is associated with the mesoscale vortex embedded in the Meiyu front; the other is related to tropical cyclones making landfall over eastern or southern China. The first one is the focus of this study. The meso-$\beta$ scale vortex (M$\beta$V) causing heavy rainfall usually forms in a col field or within a shear line associated with the mesoscale low-level jet (mLLJ). The M$\beta$V, triggered by mesoscale wind perturbation in a col field, is simulated by using a three-dimensional $\eta$-coordinate mesoscale model. This col field represents the circumstance of the "98.7" heavy rainfall event over eastern Hubei Province. The results show that the M$\beta$V triggered by wind perturbation was weak and maintained only several hours if the latent heat feedback was switched off. The wind perturbation also weakened rapidly. However, when the latent heat feedback was included, precipitation became more intense and the mLLJ and M$\beta$V quickly developed. The M$\beta$V maintained quasi-stationary during its life cycle under the stable col field.

The M$\beta$V triggered by the southwesterly perturbation was located closely to that by the northeasterly perturbation. They were both located in the weak wind region near the col point. The stronger the perturbation was, the more intense and longer the dynamic M$\beta$V lived. The 24-h accumulated precipitation in different experiments showed a similar pattern, which indicates that the relatively stable intensity and range of precipitation were the intrinsic characters of the stable col field. Furthermore, it is found that mesoscale perturbations had some impacts on the location and intensity of the rainfall. The fluctuation of large-scale LLJ to the south of the col field might produce a perturbation, causing instable stratification and rainfall within the low-level col field or shear line. The mLLJ near the rainfall was enhanced due to the latent heat feedback and then caused formation of the M$\beta$V. The stable col field provided favorable thermodynamic conditions for the formation and development of the M$\beta$V. Therefore, it is an "incubator" for M$\beta$Vs and the associated consecutive heavy rainfall.

**Key words:** col field, mesoscale vortex, mesoscale low-level jet, wind perturbation

**Citation:** Jiang Yongqiang and Wang Yuan, 2012: Numerical simulation on the formation of mesoscale vortex in col field. *Acta Meteor. Sinica*, **26**(1), 112–128, doi: 10.1007/s13351-012-0111-6.

## 1. Introduction

During the summer season in China, there exists a typical low-level col (or saddle) field over the middle and lower reaches of the Yangtze River. The col field usually consists of the western Pacific subtropical high (WPSH), the southwest vortex, the northeast low (or trough), and the Asian land high. In addition, a west-east orientated shear line is often found between the land high and the WPSH (Ding, 1992; Chen et al., 1998). In the Meiyu season, a series of mesoscale weather systems (MWSs) develop successively near the col point or the shear line under such a stable col field, resulting in persistent heavy rainfalls. Based on the observational data analysis, Zhang et al. (2004) classified the heavy Meiyu rainfall over the Yangtze River basin into three types: meso-$\beta$ scale convective rainstorm embedded in the Meiyu front,

Supported by the China Meteorological Administration Special Public Welfare Research Fund (GYHY200906011) and the National Natural Science Foundation of China (40921160382 and 40905021).

*Corresponding author: yuanasm@nju.edu.cn.

nascent-cyclone-induced heavy rainfall east of 115°E, and persistent heavy rainfall ahead of the upper-level deep trough in the upper reaches of the Yangtze River. The first type of rainfall is somewhat different from that produced by the mesoscale convective complex (MCC) defined by Maddox et al. (1979). The latter usually leads to rainstorms in spring and summer in the US. The meso-$\beta$ scale convective system (M$\beta$CS) in China is characterized by deep convection. During the active periods of Meiyu from June to July 1998, accumulated precipitation produced by the M$\beta$CS embedded within the Meiyu front takes 60%–70% of the total precipitation (Zhang et al., 2004).

The most typical Meiyu-front-induced extremely heavy rainfall event occurred over eastern Hubei Province during 20–22 July 1998 (the "98.7" event). The torrential rain was mainly triggered by a meso-$\beta$ scale vortex (M$\beta$V) which formed near the col point of a col field over eastern Hubei (Xu and Gao, 2002). Figure 1a shows the composite 700-hPa flow field from 16 to 26 July 1998, obtained by using the digital filter composite method based on Lanczos window function (Hamming, 1989; Lynch and Huang, 1992). The $0.5°\times0.5°$ resolution GAME (GEWEX Asian Monsoon Experiment; GEWEX: Global Energy and Water cycle Experiment) reanalysis data at 6-h intervals were utilized. The composite field has eliminated the irrational high-frequency noise, and therefore shows more clearly the weather situation associated with this rainfall event. A col field can be found near eastern Hubei and the col point is located near Wuhan City.

There appears another typical col pattern during summer in China when a tropical cyclone makes landfall on the coastal area. The col pattern consists of the tropical cyclone, the WPSH, the Asian land high, and a northern trough. Heavy rainfall often occurs in the col field. Figure 1b shows the 700-hPa flow field at 0000 UTC 6 July 2001. It is seen that a col field formed over eastern China when a severe rainstorm hit Shanghai with 24-h accumulated precipitation exceeding 200 mm. In this case, the WPSH ridge was situated around 25°N, and Typhoon Utor lay on the sea side of southern China. Jiang et al. (2004) indicated by numerical simulation that the M$\beta$V which produced the heavy rainfall formed at the col point under the influence of the southerly jet to the south of Shanghai.

For a long time, most studies focused on frontogenesis in the col field. Petterssen (1936) discussed the frontogenesis and frontolysis by use of the frontogenesis function. It is shown by analyzing the influence of the horizontal movement term that the deformation field is the most favorable flow field for frontogenesis. Sawyer (1956) and Eliassen (1962) proposed the concept of dynamic frontogenesis. They analyzed the impact of geostrophic and non-geostrophic deformation on frontogenesis, and the dynamic processes of non-geostrophic transverse secondary circulation.

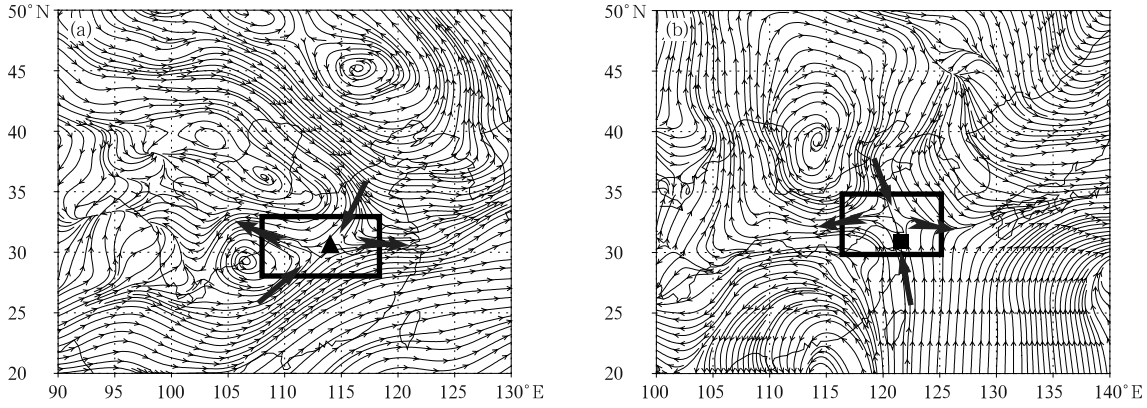


**Fig. 1.** Typical 700-hPa col patterns during summer in China. (a) The composite 700-hPa flow field from 16 to 26 July 1998 in Meiyu season and (b) the flow field before the landfall of Typhoon Utor at 0000 UTC 6 July 2001. The symbols "▲"and "■" denote the locations of Wuhan and Shanghai, respectively. The rectangle frames denote the region of cols, and the heavy arrows denote the flow at dilatation and contraction axes.

These studies promoted the development of the frontogenesis theory. According to this theory, frontogenesis secondary circulation starts at the beginning of a dynamic process when the horizontal potential temperature gradient increases near the dilatation axis in the deformation flow.

The aforementioned studies all focused on synoptic scale frontogenesis while frontogenesis associated with MWS which may result in torrential rainfall has been less investigated. With the development of mesoscale models, some studies on the formation of mesoscale vortex took advantage of the high-resolution model output data. Zhang and Fritsch (1988) indicated by numerical simulation of a squall line over Oklahoma during 7–8 July 1982 that the quasi-stationary nature of the MCS was related to the quasi-stationary low-level horizontal deformation field. The vortex formed in the deformation field and tended to be long lived because of the weak shearing environment along the deformation axis. Long et al. (2006) indicated by analyzing the structure and evolution of a meso-$\beta$ scale system that caused Meiyu frontal rainstorm during 18–19 June 2002 that two meso-$\beta$ scale systems were located in the dilatation axis of a col field in the lower troposphere.

Many observational studies have shown that there is a close relationship between heavy rainfall and the low-level jet (LLJ) (Akiyama, 1973a, b; Matsumoto, 1973; Ninomiya and Akiyama, 1974; Tao, 1980; Sun and Zhai, 1980; Chen, 1983; Chen and Yu, 1988; Tao et al., 2001; Xu and Sun, 2003). The LLJ may impact strongly the onset of heavy rainfall. The simulation case study of heavy rainstorms along the Meiyu front during 12–13 June 1991 by Chen et al. (1998) showed that the heavy precipitation that occurred in the southeastern part of a meso-$\alpha$-scale low in the 850-hPa col field was associated with a mesoscale LLJ (mLLJ) with speeds in excess of 16 m $s^{-1}$ to the south. The mLLJ was particularly important in bringing warm and moist air to support the development of the rainstorms, and the jet remained highly ageostrophic even at the storms' mature stage. Chen et al. (2005) investigated the characteristics of LLJs below 600 hPa over northern Taiwan in the Meiyu season and discussed the frequency, vertical structure, and spatial and temporal distributions of LLJs related to the onset of heavy precipitation. It is found that before and near the onset of severe heavy rainfall in northern Taiwan, there was a 94% chance that an LLJ would be present over an adjacent region at 850 hPa, and 88% at 700 hPa. Some studies indicated that an LLJ was usually observed prior to heavy rainfall and weakened after the heavy rainfall (Chen and Chi, 1978; Chen and Yu, 1988; Ding, 1992). Many studies analyzed the structure and formative reasons of LLJ (Akiyama, 1973c; Matsumoto, 1973; Ninomiya and Akiyama, 1974; Chen, 1982; Chou et al., 1990; Chen et al., 2006; Muñoz et al., 2008; Whyte et al., 2008; Cuxart, 2008; Shapiro and Fedorovich, 2009; Parish, 2010). The observational facts and numerical simulations reveal that most of the foregoing heavy rainfalls associated with LLJs form in the col field and are related to M$\beta$V, indicating close relationships between col field, LLJ and the M$\beta$V. However, there are two problems to be solved: (1) How does the M$\beta$V form? (2) Have the LLJ and the col field had any impact on the formation of the M$\beta$V?

In this study, a mesoscale $\eta$-coordinate numerical model is employed to simulate the formation of an M$\beta$V in col field with the influence of different wind perturbations. The evolution of the M$\beta$V and associated rainfall is analyzed. Section 2 briefly describes the model and the methodology used in this study. Section 3 gives the simulation results. Conclusions and discussion are given in the last section.

## 2. Model and experimental design

### *2.1 Model description*

The model used for this study is an improved version of the three-dimensional $\eta$-coordinate mesoscale model designed by Yu et al. (1994). The model uses the IAP-GCM (Institute of Atmospheric Physics General Circulation Model) dynamic frame which maintains the complete energy conservation (Zeng and Zhang, 1981). The Betts cumulus parameterization scheme (Betts, 1986) for subgrid-scale convection and the saturation condensation function for grid-scale

precipitation are chosen to represent precipitation physics. The Blackada high-resolution PBL (planetary boundary layer) scheme (Zhang and Anthes, 1982) is used to calculate the vertical fluxes of latent heat, sensible heat, and momentum in the PBL. The step-topography of the model uses the envelope method (Wallace et al., 1983) based on global 5′ initial topography data. A detailed description of the model is given in Jiang et al. (2002).

The model initial conditions are obtained by objectively analyzing radiosonde and surface observations archived at the National Meteorological Center of China using an optimal interpolation scheme. Figure 2 shows the model domain which covers 221 (longitude) × 241 (latitude) × 23 (vertical) grids with the horizontal resolution of 0.25°×0.25° (about 18 km for E-grid in midlatitudes). The model top is at 100 hPa.

### *2.2 Experimental design*

Many studies suggested that the M$\beta$CS associated with heavy rainfall is related to large-scale LLJ. LLJ is usually observed prior to significant convection, and the intensity of LLJ decreases after the heavy rainfall (Chen and Chi, 1978; Chen and Yu, 1988; Ding, 1992). The perturbation of large-scale LLJ may directly triggers heavy rainfall (Chen, 1982; Chen, 1983; Chen et al., 1998). Matsumoto (1973) and Ninomiya and Akiyama (1974) suggested that LLJ results from the downward mixing of southwesterly momentum from upper levels by convection. But Chen (1982) argued that the LLJ is produced by thermal

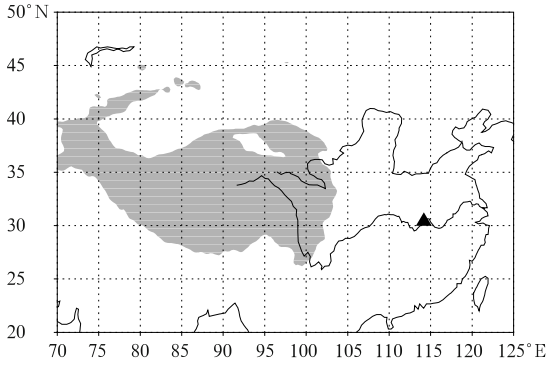


**Fig. 2.** Model domain. Shadings denote the model terrain higher than 3000 m. The symbol "▲" denotes the location of Wuhan City of Hubei Province.

wind adjustment that occurs in the entrance region of the upper-level jet. Chen and Yu (1988) suggested by an observational study that an LLJ might form to the south of the heavy rainfall, and the reversed secondary circulation driven by convective latent heating is a possible formation mechanism for the LLJ. Other observational studies and numerical simulations also gave a similar viewpoint (Chen et al., 1998, 2000; Chou et al., 1990; Chen et al., 2006). The aforementioned studies suggested that the LLJ may be related to the latent heating.

During the "98.7" event, there existed a stable col filed over eastern Hubei Province. Observational and numerical studies have investigated in detail about the large-scale pattern, mesoscale system, and the formative mechanism of the rainstorm (Hu et al., 2001; Bei et al., 2002; Xu and Gao, 2002; Jiang and Wang, 2010). The mesoscale system leading to the rainstorm has a 12-h life cycle and a 100- to 200-km horizontal scale, which are characteristic of a typical M$\beta$V (Bei et al., 2002). Jiang and Wang (2010) suggested that the mLLJ to the south of the rainstorm may be responsible for the M$\beta$V.

It is assumed that the LLJ and the associated perturbations must be very weak, and the M$\beta$V may not form if the latent heat feedback process in the model is closed. A pure stable col field may be taken as a background to study the dynamic formative mechanism of the M$\beta$V in the "98.7" event. In such a stable col filed, the formation of M$\beta$V can be numerically simulated with different mesoscale wind perturbations.

It is shown in Fig. 1a that the inflows at contraction axis consist of mainly southwesterly to the south and northeasterly to the north of the col field, so the mesoscale southwesterly perturbation (SWP) and northeasterly perturbation (NEP) are imposed in the numerical experiments. The experiments are summarized in Table 1. All the experiments have the same initial condition. The simulations cover a 48-h period from 0000 UTC 21 to 0000 UTC 23 July 1998. In the first experiment (EXP1), the latent heat feedback is switched off to obtain the pure col field. Other experiments are conducted with different location and intensity of wind perturbations which are added to

**Table 1.** Summary of numerical experiments

| Experiment | Latent heat feedback | Wind direction of perturbation | Central location of perturbation | Maximum wind speed of perturbation (m $s^{-1}$) |
|---|---|---|---|---|
| EXP1 | No | No | No | No |
| EXP2 | No | Southwest | 31°N, 114.25°E | 25 |
| EXP3 | Yes | Southwest | 31°N, 114.25°E | 25 |
| EXP4 | No | Northeast | 33°N, 114.25°E | 25 |
| EXP5 | Yes | Northeast | 33°N, 114.25°E | 25 |
| EXP6 | No | Southwest | 31°N, 114.25°E | 35 |
| EXP7 | Yes | Southwest | 31°N, 114.25°E | 35 |

the model at $t = 17$ h.

Because the structures of LLJ and M$\beta$V are quite different at low levels, it is difficult to give a perturbation same as the observation. However, the purpose of these experiments is to simulate the formation of M$\beta$V at one level but not all the levels. It is successful if an M$\beta$V is simulated at 700 hPa. Thus, wind perturbations with the same structure at 8–17 model levels (about 600 to 850 hPa) are prescribed. The perturbation wind ($u'$, $v'$) is defined as:

$$u' = U_0 \mathrm{e}^{-cr^2}, \quad v' = V_0 \mathrm{e}^{-cr^2}, \tag{1}$$

where $U_0$ and $V_0$ are the maximum zonal and meridional components of wind speed at the center of perturbation, respectively. Variable $r$ is the distance apart from the perturbation center, and $c$ is the attenuation coefficient of the wind speed, which is given a constant value of 0.15.

It is necessary to give a perturbation geopotential height $h'$ to balance the perturbation wind. The geostrophic theory is used as a constraint condition.

$$u' = -g\partial h'/f\partial y, \tag{1a}$$

$$v' = g\partial h'/f\partial x, \tag{1b}$$

where $g$ and $f$ are the gravitational constant and the Coriolis parameter, respectively. Equations (1a) and (1b) are differentiated to obtain

$$\nabla^2 h' = f\zeta'/g, \tag{2}$$

where $\zeta'$ is the vertical component of perturbation relative vorticity, and $\zeta' = \partial v'/\partial x - \partial u'/\partial y$. Equation (2) is a Possion Equation. Given a boundary condition and an initial wind field, the initial perturbation geopotential height (Fig. 3) can be calculated by use of a successive over-relaxation iterative method.

## 3. Results

### *3.1 EXP1*

Figure 4 shows the 700-hPa wind stream field of EXP1. Without the latent heating, the large-scale LLJ to the southwest of Wuhan is clearly weaker than that considering the feedback of latent heat (figure omitted). A stable col field is located near eastern Hubei Province without any M$\beta$V in the col field. It is suggested that the feedback of latent heat is mainly responsible for the large-scale LLJ. Thus, a stable col field is taken as an ideal background for the following experiments with wind perturbations.

Based on the experimental design in Table 1, the mesoscale SWP and NEP are added to the ideal col

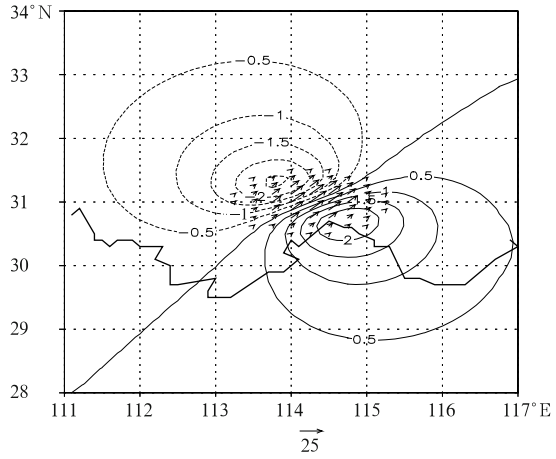


**Fig. 3.** Initial SWP (arrows; m $s^{-1}$) and geopotential height perturbation (contours; gpm).

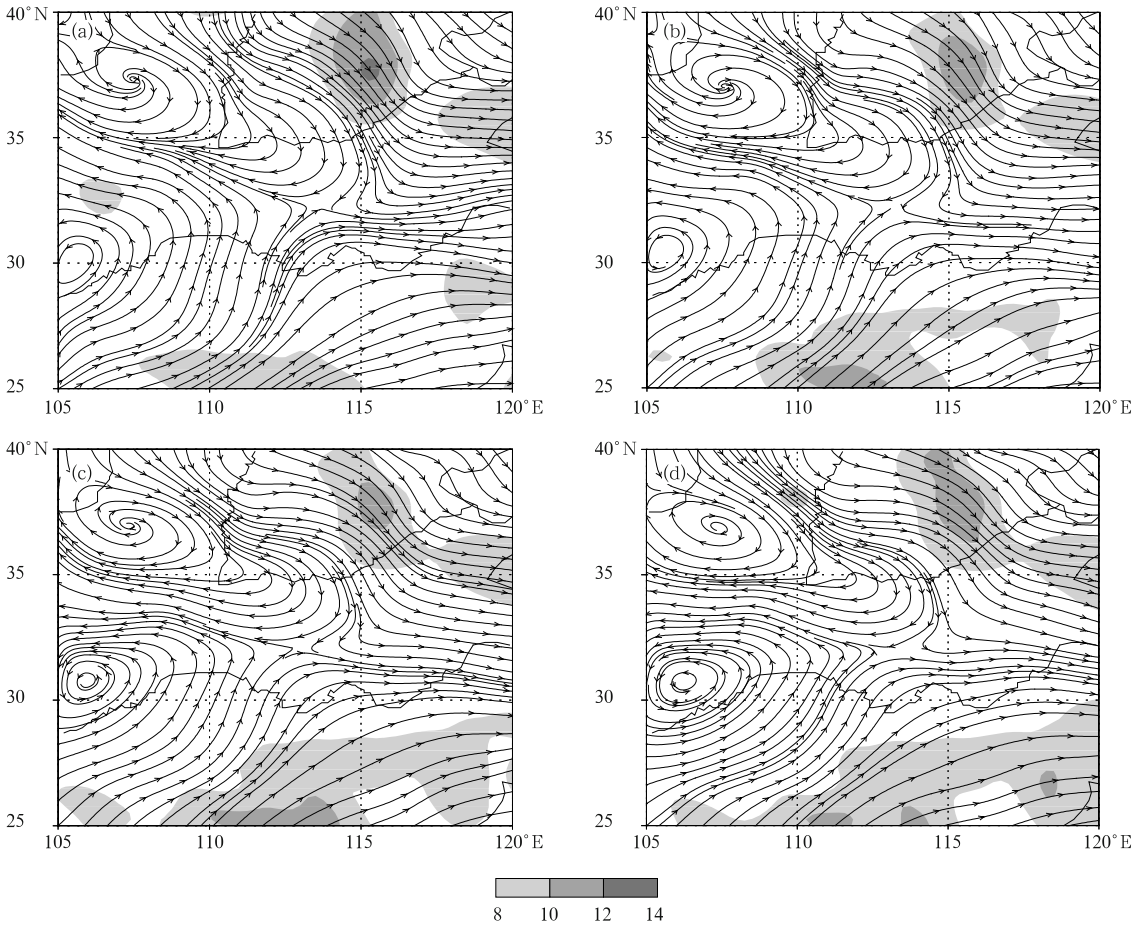


**Fig. 4.** Simulated 700-hPa streamline and wind velocity (m $s^{-1}$) of EXP1 at (a) $t$ = 17 h, (b) $t$ = 19 h, (c) $t$ = 21 h, and (d) $t$ = 23 h. Shadings denote areas with wind speed greater than 8 m $s^{-1}$.

field at $t$ = 17 h. Figure 5 shows the simulated 700-hPa streamline and wind speed fields with the perturbation superimposed on the background. Though the maximum wind speed at the center of perturbation is 25 m $s^{-1}$, the region with wind speed larger than 14 m $s^{-1}$ is quite small, and intense gradient of wind speed appears near the perturbation center. Because the background southwesterly to the south of the col field is relatively strong, the total wind speed of SWP is larger than that of NEP. The streamlines and wind speeds in the following figures are based on total winds.

### *3.2 EXP2*

Figure 6 shows the 700-hPa wind stream and wind velocity of EXP2. There is a region with wind speed exceeding 14 m $s^{-1}$ to the south of the col field at $t$ = 17 h. The streamlines have little changes at $t$ = 18 h, but a cyclonic streamline curve occurs to the north of Wuhan near the col point at $t$ = 19 h. This cyclonic curve becomes more intense during the following 2 hours, and then an M$\beta$V forms in the col field at $t$ = 21 h. The wind speed of the perturbation center quickly reduces from 25 m $s^{-1}$ at $t$ = 17 h to less than 10 m $s^{-1}$ at $t$ = 18 h, and less than 8 m $s^{-1}$ at $t$ = 21 h.

The results of EXP2 show that wind perturbation can dynamically trigger an M$\beta$V in the col field. It is suggested that the M$\beta$V may be caused by mLLJ in the col field. However, the mLLJ and M$\beta$V cannot be long lived without the latent heat feedback.

Figure 7 shows the 700-hPa relative vorticity and corresponding 1-h accumulated precipitation of EXP2. The mesoscale perturbations produce a

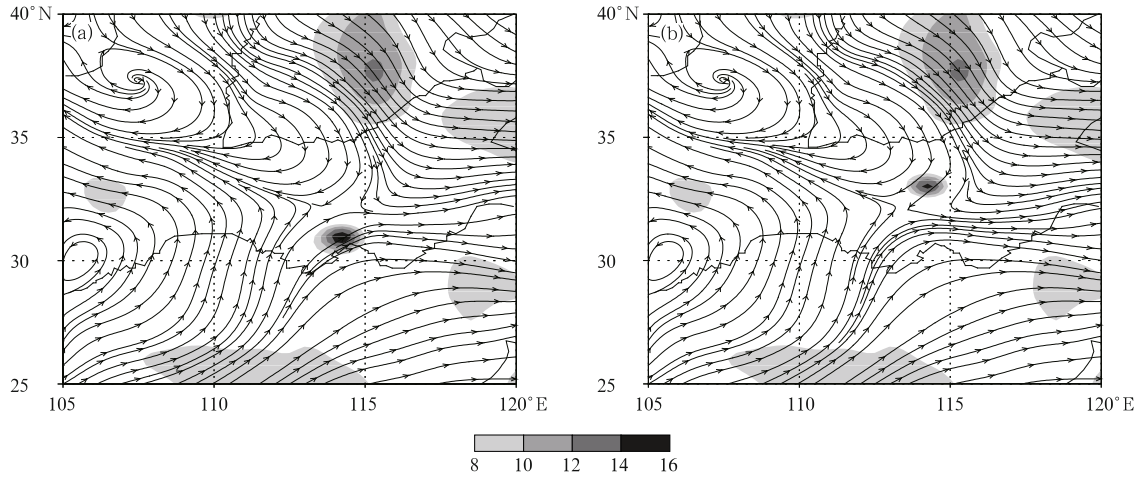


**Fig. 5.** Simulated 700-hPa streamline with (a) SWP and (b) NEP at $t$ = 17 h. Shadings denote areas with the total wind speed greater than 8 m s$^{-1}$.

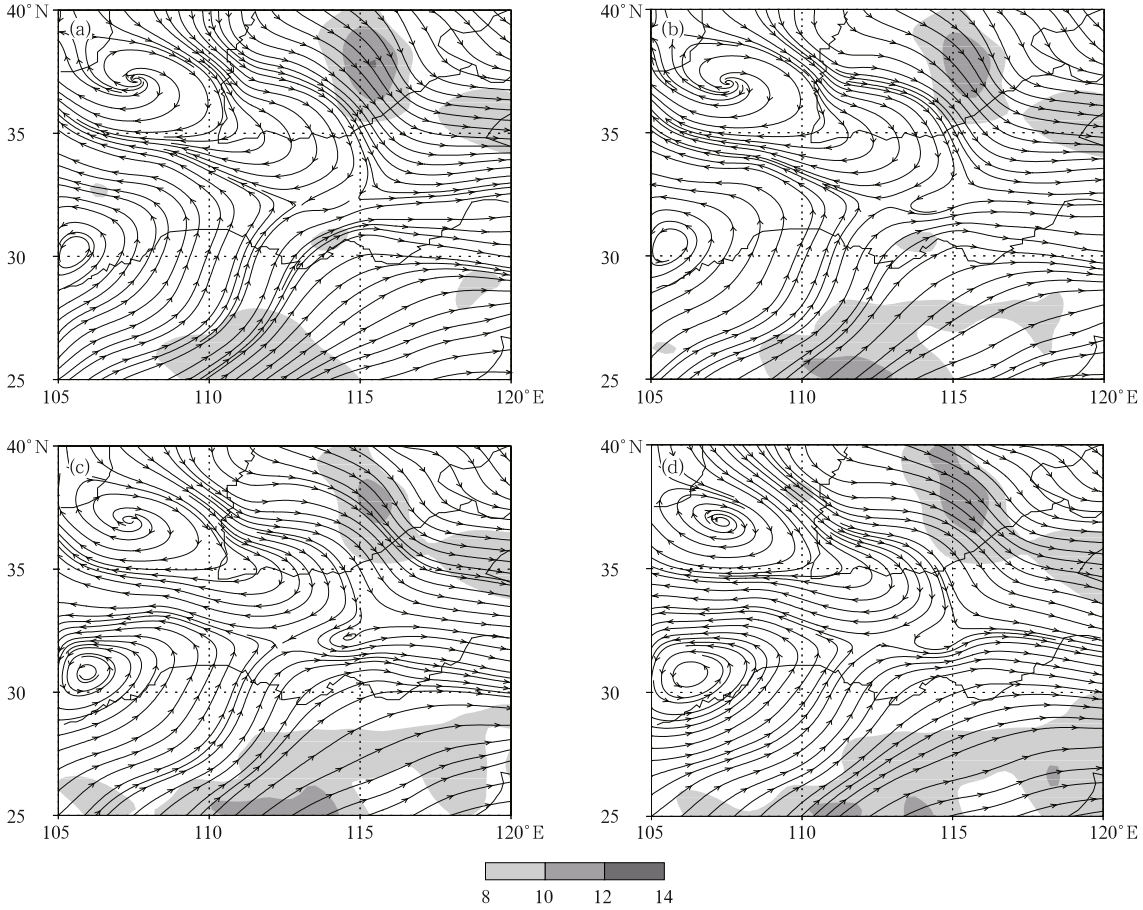


**Fig. 6.** Simulated 700-hPa streamline and wind velocity (shadings; m s$^{-1}$) of EXP2 at (a) $t$ = 18 h, (b) $t$ = 19 h, (c) $t$ = 21 h, and (d) $t$ = 23 h.

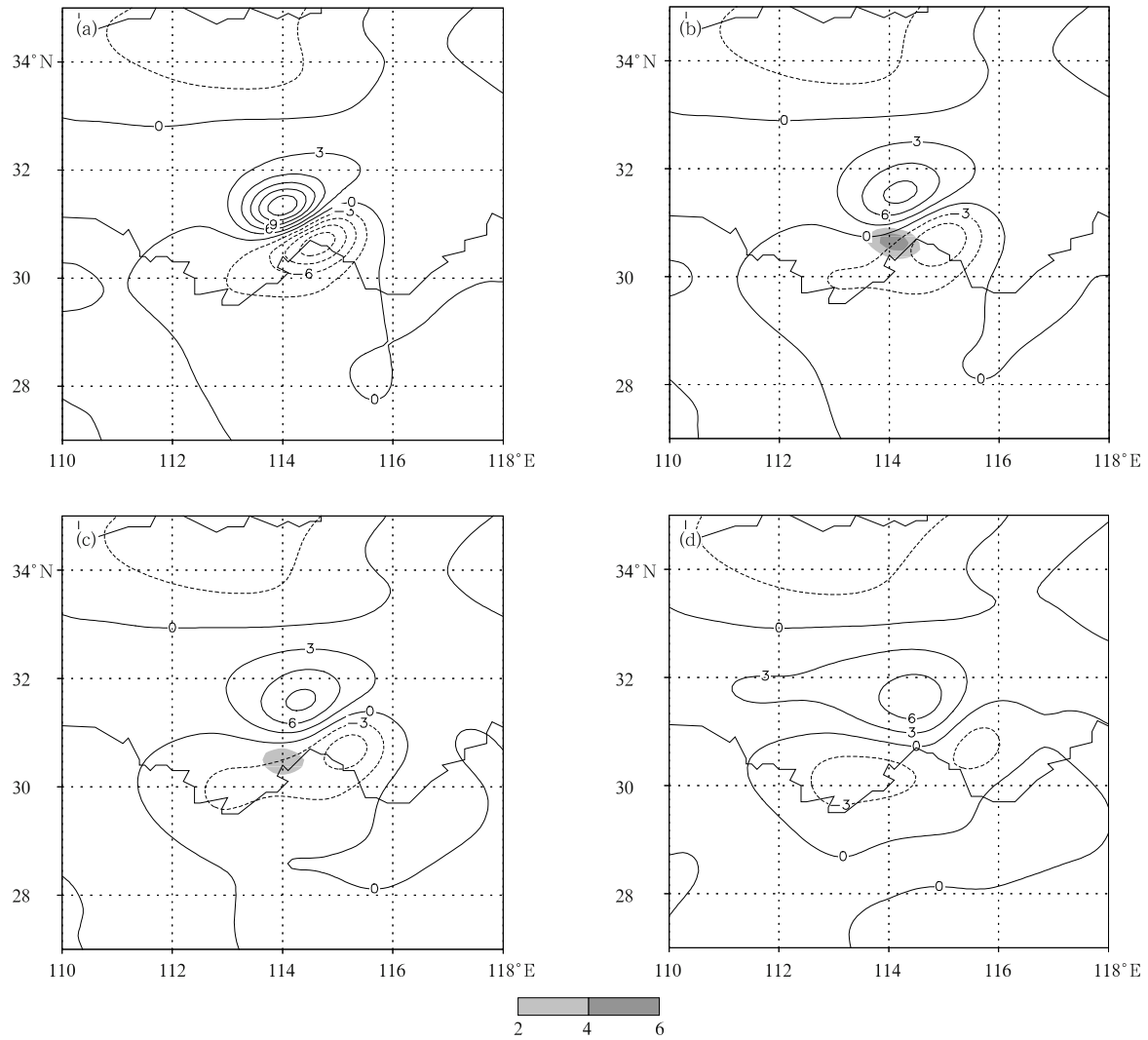


**Fig. 7.** 700-hPa relative vorticity (contours; $10^{-5}$ s$^{-1}$) and corresponding 1-h accumulated precipitation (shadings; mm) of EXP2 at (a) $t$ = 17 h, (b) $t$ = 18 h, (c) $t$ = 19 h, and (d) $t$ = 21 h.

vorticity couplet with the center vorticity value higher than $15\times10^{-5}$ s$^{-1}$ at $t$ = 17 h. However, the vorticity weakens rapidly. The value of the positive vorticity center is reduced to $9\times10^{-5}$ s$^{-1}$ at $t$ = 18 h and $6\times10^{-5}$ s$^{-1}$ at $t$ = 21 h. As the perturbation is added to the model, rainfalls appear immediately, but the precipitation is quite small when the latent heat feedback is off, and the center value of 1-h accumulated precipitation is also rapidly reduced from higher than 4 mm at $t$ = 18 h to less than 2 mm at $t$ = 21 h.

### *3.3 EXP3*

In EXP2, the M$\beta$V triggered by SWP is quite weak due to the switch-off of the latent heat feedback. It is wondered whether the mLLJ could maintain or intensify and whether the weak M$\beta$V could develop when the latent heat feedback is switched on after $t$ = 17 h. Figure 8 shows the 700-hPa streamline and wind speed fields of EXP3. The perturbation also weakens after $t$ = 17 h though the latent heat feedback is now in effect. However, an M$\beta$V forms near the col point at $t$ = 19 h. An mLLJ to the southwest of the M$\beta$V intensifies from $t$ = 20 h, and the M$\beta$V also develops. The center value of mLLJ is higher than 10 m s$^{-1}$ at $t$ = 21 h (Fig. 8b). With the intensification of the mLLJ, the size of the M$\beta$V circulation is enlarging,

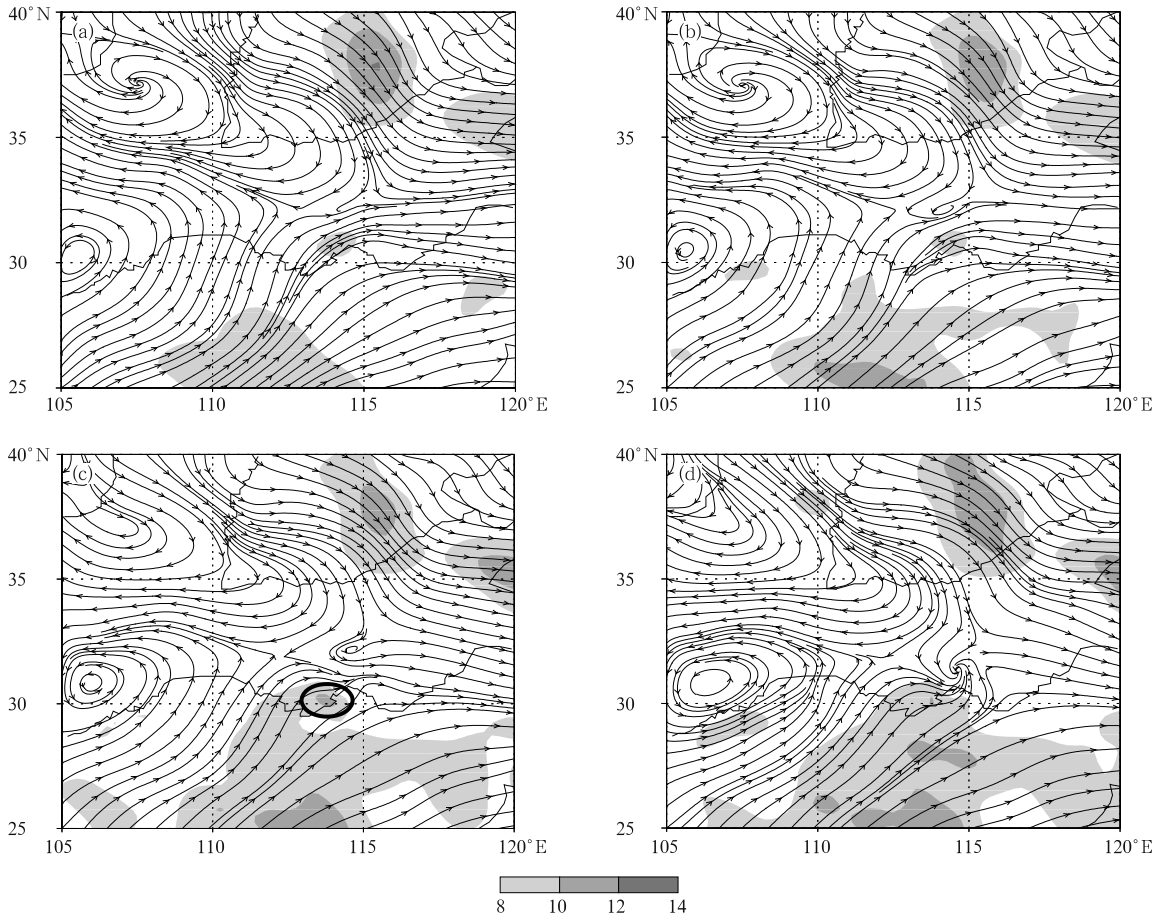


**Fig. 8.** Simulated 700-hPa streamline and wind velocity (shadings; m $s^{-1}$) of EXP3 at (a) $t$ = 18 h, (b) $t$ = 19 h, (c) $t$ = 21 h, and (d) $t$ = 23 h.

and the M$\beta$V becomes a meso-$\alpha$ vortex after $t$ = 30 h (figures omitted). The mesoscale vortex maintains quasi-stationary during its life cycle.

Figure 9 shows the 700-hPa relative vorticity and 1-h accumulated precipitation of EXP3. The vorticity pattern is the same as EXP2 before $t$ = 17 h, and the vorticity also weakens rapidly in association with light precipitation before $t$ = 19 h. However, with the latent heat feedback being turned on, the rainfall intensifies quickly from $t$ = 19 h, and the center of 1-h accumulated precipitation exceeds 40 mm from $t$ = 20 to $t$ = 22 h. At the same time, the positive vorticity becomes more intense, with the center value higher than $12\times10^{-5}$ $s^{-1}$ at $t$ = 22 h and $21\times10^{-5}$ $s^{-1}$ at $t$ = 25 h.

Some studies (Chen, 1982; Chou et al., 1990) suggested that Coriolis acceleration of the northward motion in the lower branch of the mesoscale secondary circulation induced by convective latent heat release is a possible mechanism for the formation of the LLJ. Chen et al. (1998) revealed that latent heat release is crucial for the development of the rainstorm, the mLLJ, the mesolow, the rapid spin up of vorticity, and the Meiyu frontogenesis. The simulation results of EXP3 also reveal a close relationship of these factors.

### *3.4 EXP4*

The configuration of EXP4 is the same as that of EXP2 except with the NEP as shown in Fig. 5b. The latent heat feedback is not considered either. Figure 10 shows the 700-hPa streamlines and wind velocity.

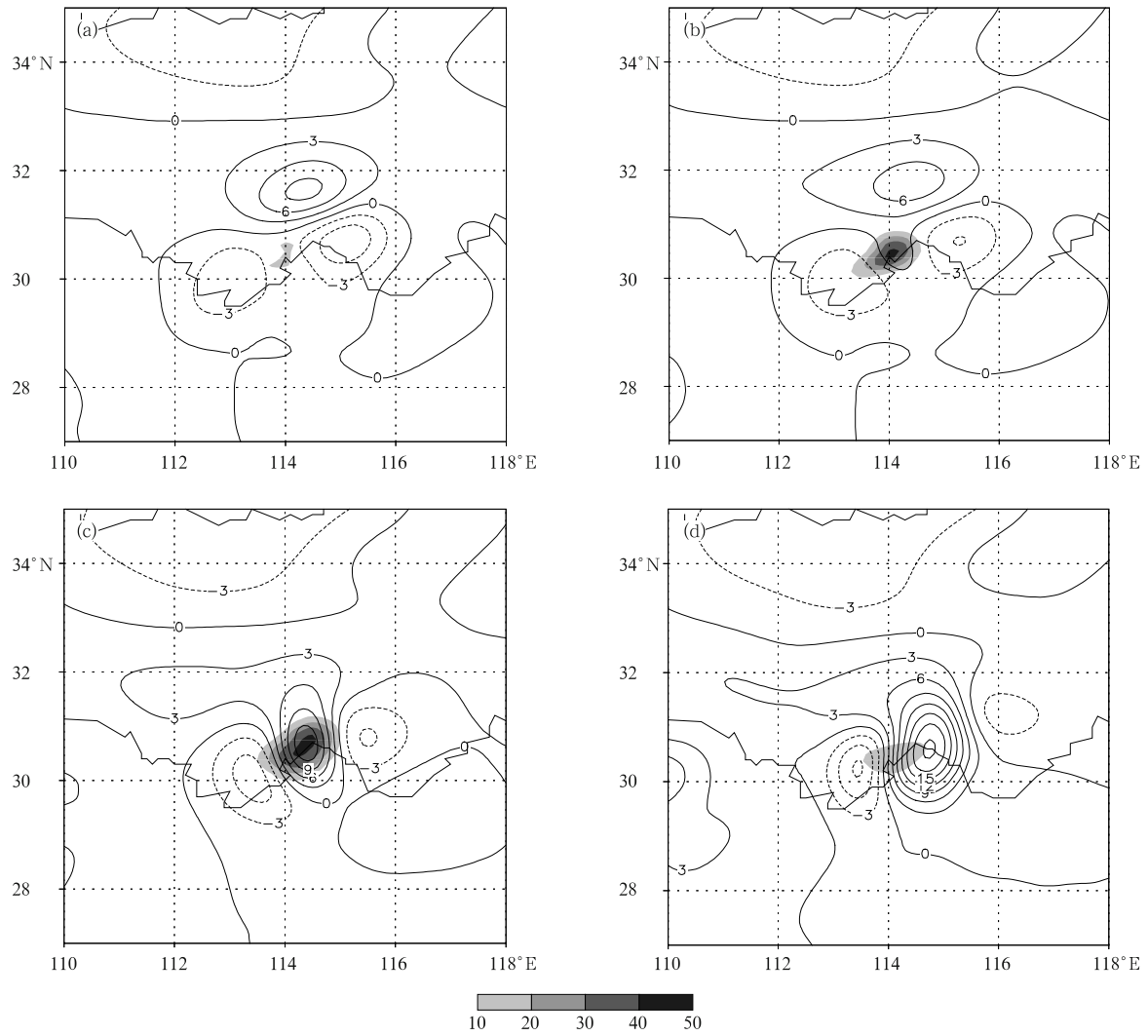


**Fig. 9.** 700-hPa relative vorticity (contours; $10^{-5}$ $s^{-1}$) and corresponding 1-h accumulated precipitation (shadings; mm) of EXP3 at (a) $t$ = 19 h, (b) $t$ = 20 h, (c) $t$ = 22 h, and (d) $t$ = 25 h.

The streamlines also have little changes at $t$ = 18 h but an M$\beta$V forms in the col field at $t$ = 19 h. The location of the M$\beta$V is close to that of EXP2, and the duration of the M$\beta$V is also 2 h. The 700-hPa relative vorticity and corresponding 1-h accumulated precipitation fields of EXP4 (figure omitted) show that a vorticity couplet with positive vorticity to the southeast and negative vorticity to the northwest of the perturbation center forms in the col field. The vorticity also weakens rapidly. To the north of the col field, there is no precipitation near the NEP.

### *3.5 EXP5*

EXP5 is similar to EXP4 but the latent heat feedback is turned on after $t$ = 17 h. Figure 11 shows the 700-hPa streamlines and wind velocity of EXP5. The M$\beta$V with the same location to that of EXP4 is triggered at $t$ = 19 h. The mLLJ to the south of the col field becomes intense after $t$ = 21 h, and the M$\beta$V also develops after $t$ = 23 h.

The simulated 700-hPa relative vorticity and corresponding 1-h precipitation of EXP5 is shown in Fig. 12. Though the positive vorticity near the perturbation is quite strong, there is no precipitation there. The rainfall occurs to the south of the col field with precipitation exceeding 10 mm. It indicates that the rainfall is triggered by the perturbation under the favorable circumstance where warm and moist air is

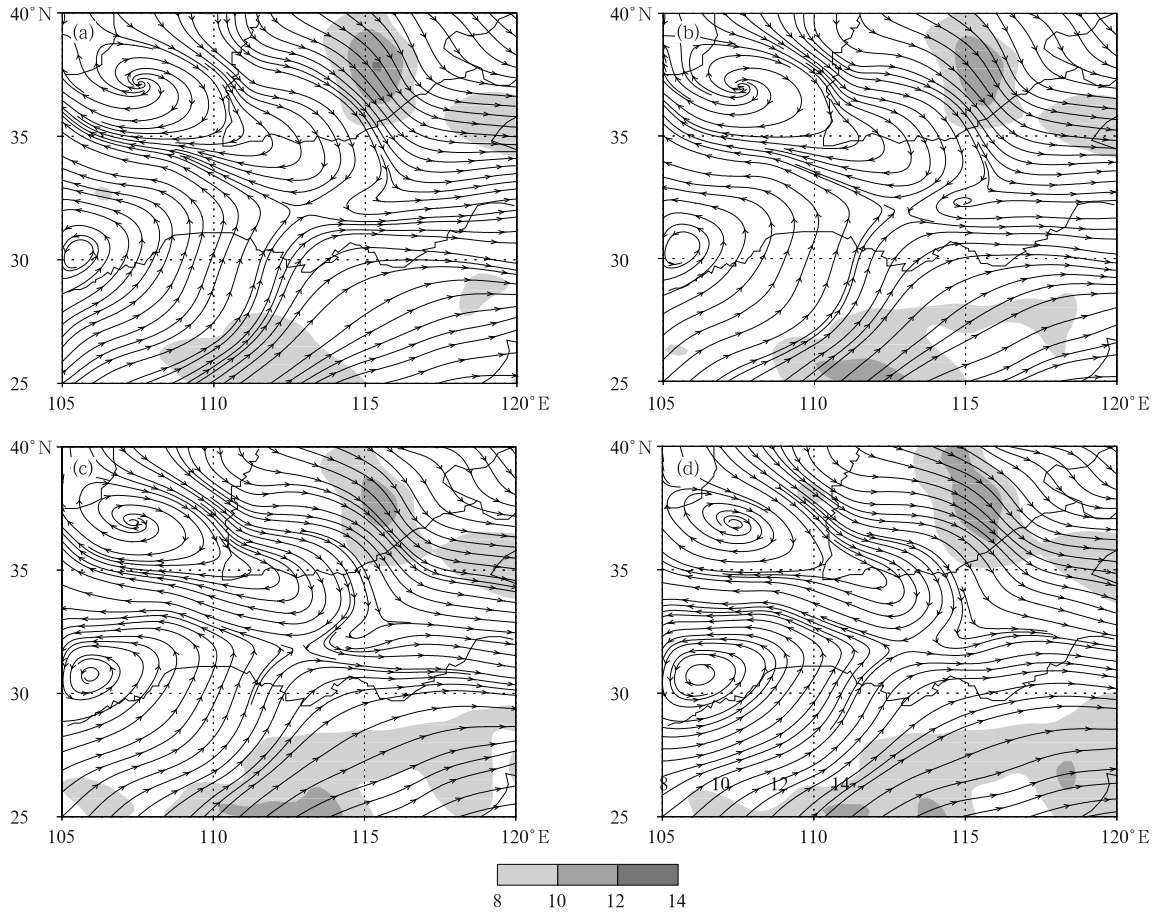


**Fig. 10.** Simulated 700-hPa streamline and wind velocity (shadings; m $s^{-1}$) of EXP4 at (a) $t$ = 18 h, (b) $t$ = 19 h, (c) $t$ = 21 h, and (d) $t$ = 23 h.

transported by the southwesterly flow. The 1-h precipitation increases to higher than 40 mm at $t$ = 20 h, following the intensification of positive vorticity in the rainfall region. The rainfall range extends further with a maximum 1-h precipitation at $t$ = 22 h when the perturbation positive vorticity emerges into the positive vorticity in the rainfall region, with an enhanced positive vorticity center value higher than $12\times10^{-5}$ $s^{-1}$. The rainfall region is located slightly south to those of EXP3. The positive vorticity intensifies with a maximum center value higher than $21\times10^{-5}$ $s^{-1}$ at $t$ = 25 h due to the intensive precipitation. It is shown that the location, range, and intensity of the rainfall in EXP5 are close to that of EXP3, with the latent heat feedback in the stable col field. The perturbation could have played a distinct role in deciding the location and intensity of the rainfall.

### *3.6 EXP6 and EXP7*

For the purpose of comparing the effects of different perturbation intensity on the M$\beta$V and the associated rainfall, EXP6 is configured in the same way as EXP2 but with a more intense perturbation. The maximum wind speed of the perturbation is 35 m $s^{-1}$. Figure 13 shows that the M$\beta$V forms at $t$ = 18 h for the intensive perturbation, earlier than that of EXP2. The M$\beta$V has a maximum intensity which is clearly stronger than that of EXP2 at $t$ = 21 h, and it lasts for 4 h. This suggests that the stronger the mesoscale perturbation, the more intense and longer lived the dynamic M$\beta$V.

EXP7 is the same as EXP3 but with a stronger wind perturbation. The M$\beta$V in EXP7 is quite similar

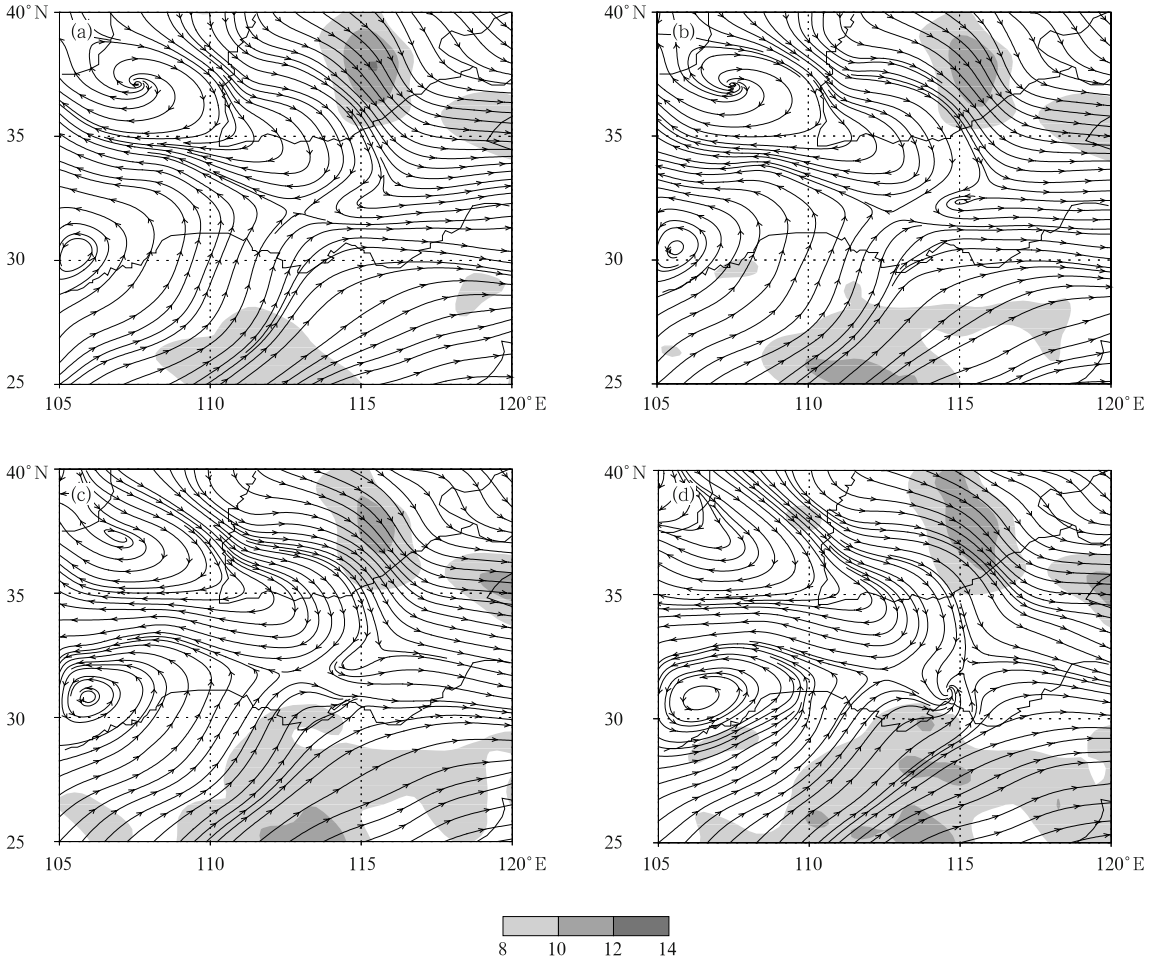


**Fig. 11.** As in Fig. 10, but for EXP5.

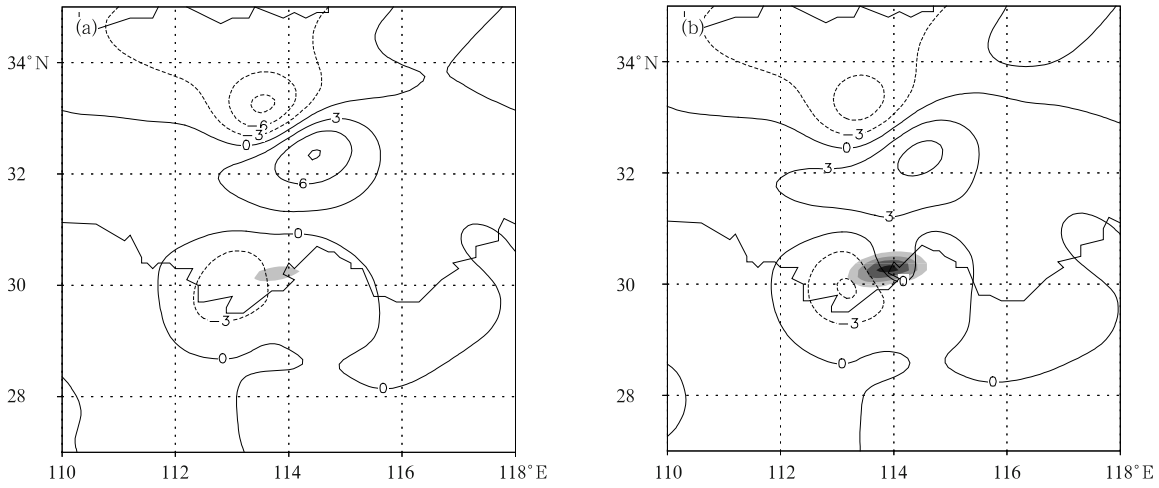


**Fig. 12.** Simulated 700-hPa relative vorticity (contours; $10^{-5}$ $s^{-1}$) and 1-h accumulated precipitation (shadings; mm) of EXP5 at (a) $t$ = 19 h, (b) $t$ = 20 h, (c) $t$ = 22 h, and (d) $t$ = 25 h.

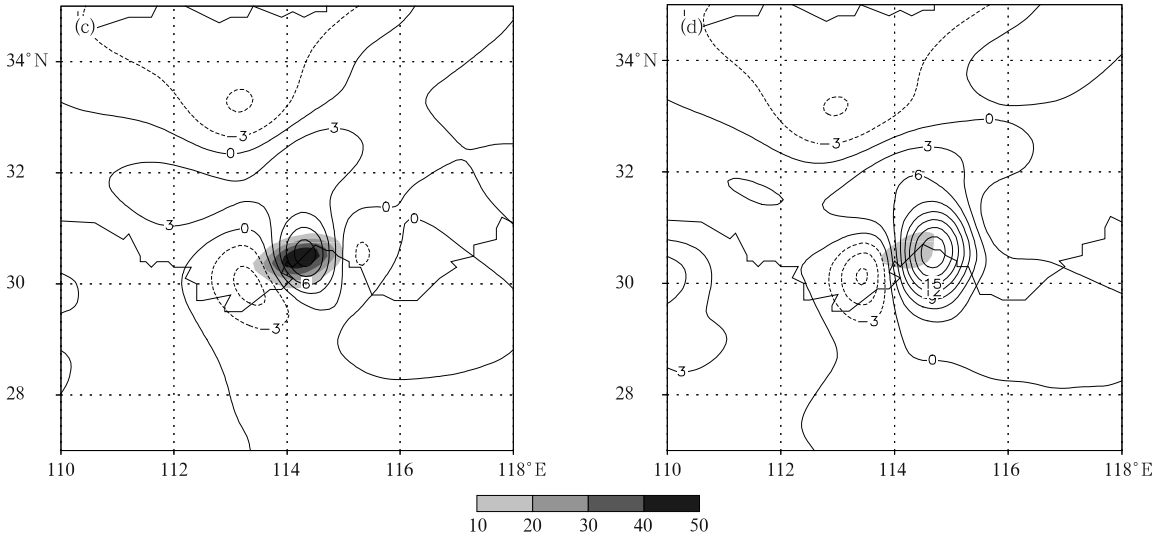


**Fig. 12.** (Continued.)

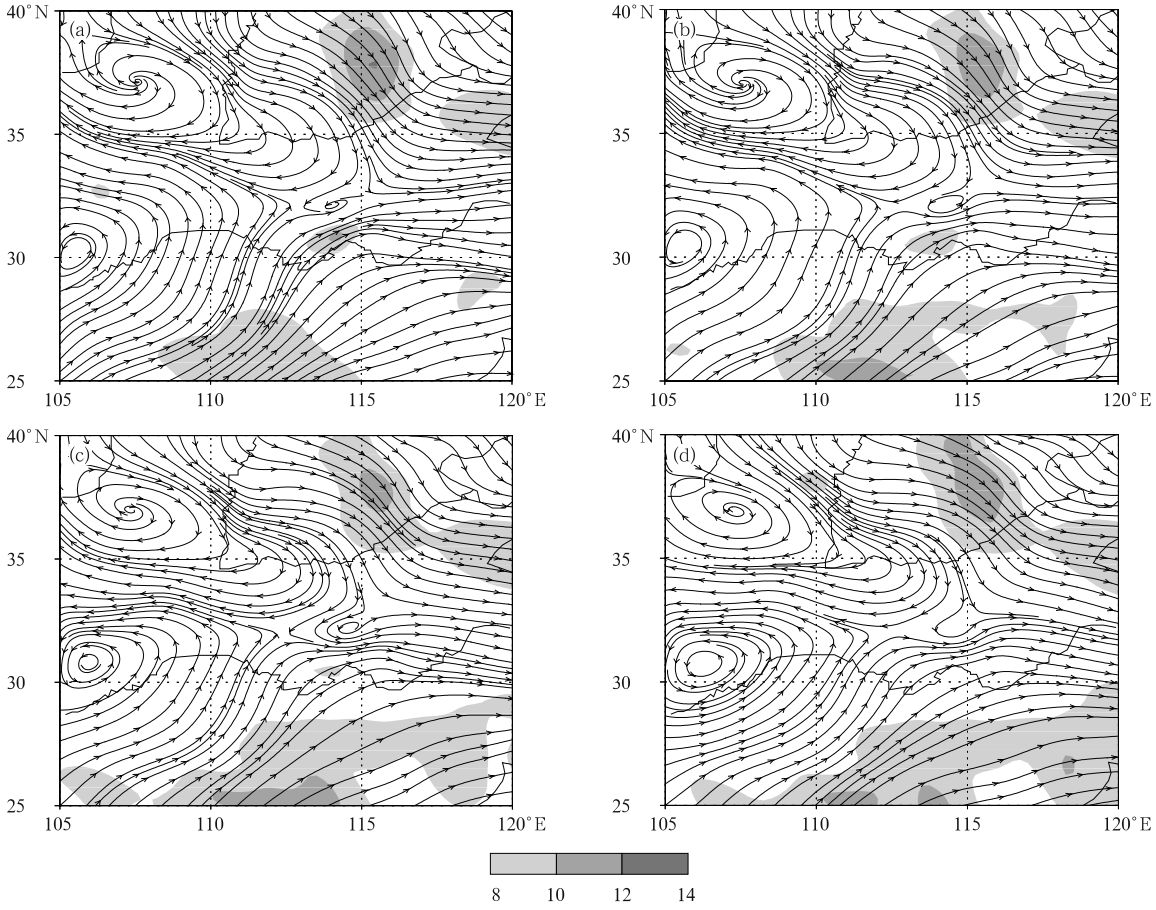


**Fig. 13.** Simulated 700-hPa streamline and wind velocity (shadings; m $s^{-1}$) of EXP6 at (a) $t = 18$ h, (b) $t = 19$ h, (c) $t = 21$ h, and (d) $t = 23$ h.

to that in EXP3 under the effect of latent heat release (figures omitted).

### *3.7 Comparison of 24-h precipitation*

Comparison of 24-h accumulated precipitation between EXP3, EXP5, and EXP7 is shown in Fig. 14. The observed torrential rainfall in Wuhan is well simulated in EXP3 and EXP5. On the whole, the structure of the simulated rainfall of EXP3 is similar to that of EXP5, but the precipitation of EXP3 is 40 mm more to the north and 30 mm less to the south of Wuhan than that of EXP5 (Fig. 14c). In other words, the central location of the simulation rainfall with SWP is located to the north of that with NEP. The differences of simulated 24-h precipitation between EXP7 and EXP3 are quite small, and the maximum difference is only about 9 mm (Fig. 14d). The strengthened SWP leads to a northward heavy rainfall region. The simulation results indicate that the rainfall in the stable col field also has relative stable characters, which may be the intrinsic character of the stable col field. The wind perturbation could trigger the onset of rainfall in the warm and moist environment. Different locations and intensities of the wind perturbation exert little effect on the whole distribution of the precipitation, but they could impact on the central location and

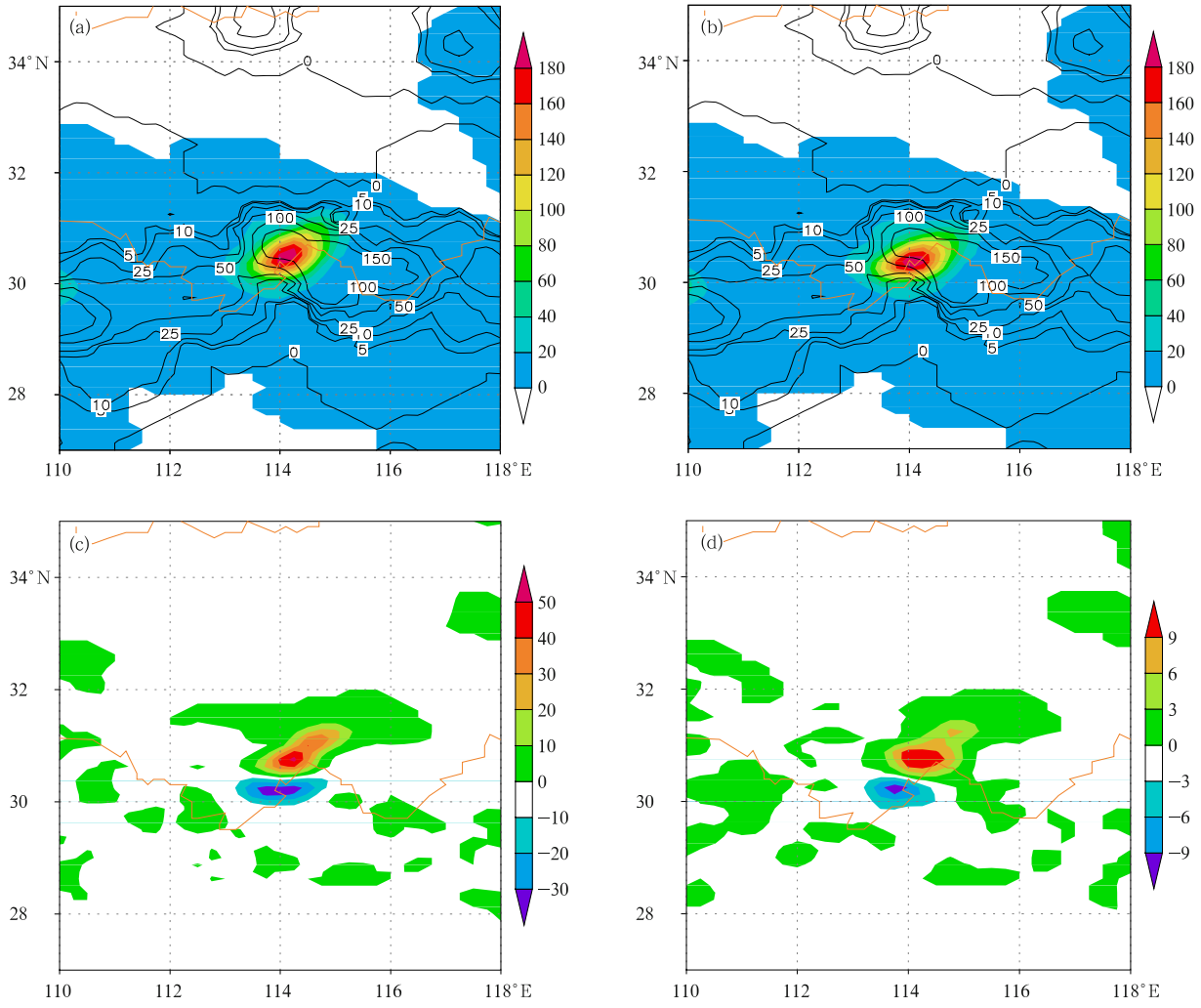


**Fig. 14.** Observed and simulated 24-h accumulated precipitation. (a) EXP3, (b) EXP5, (c) EXP3 minus EXP5, and (d) EXP7 minus EXP3. The contours and shadings denote observed and simulated precipitation (mm), respectively.

intensity of the rainfall to a certain extent.

## 4. Conclusions and discussion

The above simulations show that mesoscale wind perturbations could trigger M$\beta$V in a weak background. This was confirmed by observations and simulations in which the M$\beta$Vs responsible for heavy rainfalls usually formed in weak wind backgrounds such as col fields (deformation fields) and shear lines (Zhang and Fritsch, 1988; Xu and Gao, 2002; Jiang et al., 2004; Long et al., 2006). The formative reason of the M$\beta$V triggered by mesoscale wind perturbation can be explained by a theory that a dot vorticity can form a cyclonic (or anticyclonic) circulation (e.g., Brown, 1991), i.e., the perturbation leads to a vorticity couplet, and the positive vorticity which is close to the col point triggers the dynamic M$\beta$V in the col field. The intensity of the dynamic M$\beta$V depends on the intensity of perturbation. The dynamic M$\beta$V should not be long lived, but it could intensify with the effect of latent heat release.

In summer monsoon season of China, there is often a southwesterly LLJ to the south of the col field, which propagates along the axis of LLJ. The wind speed fluctuation of the LLJ's core produces a perturbation which tends to move toward the col point or the dilatation axis of the col field where the M$\beta$V may be easily triggered. Furthermore, it has been pointed out that the LLJ to the south of the col field transports low-level warm and moist air northward, and produces a convectively unstable layer (Chen, 1983). Once precipitation is produced, the M$\beta$V may enhance due to the latent heat release, and then the positive feedback may lead to heavy rainfall.

When different wind perturbations move toward the stable col field, they could dynamically trigger M$\beta$Vs located closely, indicating that the weak wind circumstance such as the col field is favorable for the formation of M$\beta$V. The weak background is also usually found along a low-level shear line at 850 or 700 hPa. It is verified by Fu et al. (2004) that four meso-$\beta$ scale cyclones (called "vortex train") observed by GMS-5 IR images formed along the low-level shear line. The vortex train along the shear line was also simulated by MM5 with a 10-km horizontal resolution (Zhai et al., 2003; they called it "vortex group") and by a numerical simulation study on a severe storm in Jiangxi Province in 2003 (Jiang and Song, 2010). Though the range, intensity, and central location of the rainstorm have some differences with different wind perturbations, the overall structures of the rainfall are quite similar. The stable col field provides a favorable thermodynamic background for the formation and development of M$\beta$V. Therefore, it is an "incubator" for M$\beta$Vs and associated consecutive heavy rainfall.

***Acknowledgments.*** The GAME reanalysis data were provided by the Japan Meteorological Agency and the Earth Observation Research Center/National Space of Development Agency of Japan.

## REFERENCES

Akiyama, T., 1973a: The large-scale aspects of the characteristic features of the Baiu front. *Paper Meteor. Geophys.*, **24**, 157–188.

——, 1973b: Frequent occurrence of heavy rainfall along the north side to the low-level jet stream in the Baiu season. *Paper Meteor. Geophys.*, **24**, 379–388.

——, 1973c: Ageostrophic low-level jet stream in the Baiu season associated with heavy rainfalls over the sea area. *J. Meteor. Soc. Japan*, **51**, 205–208.

Bei, N. F., S. X. Zhao, and S. T. Gao, 2002: Numerical simulation of a heavy rainfall event in China during July 1998. *Meteor. Atmos. Phys.*, **80**, 153–164.

Betts, A. K., 1986: A new convective adjustment scheme. Part I: Observational and theoretical basis. *Quart. J. Roy. Meteor. Soc.*, **112**, 677–691.

Brown, R. A., 1991: *Fluid Mechanics of the Atmosphere*. Academic Press, INC., San Diego, California, 489 pp.

Chen George Tai-jen and Chi Shui-Shang, 1978: On the mesoscale structure of Meiyu front in Taiwan. *Atmos. Sci.*, **5**(1), 35–47. (in Chinese)

Chen, G. T. J., 1983: Observational aspects of the Meiyu phenomena in subtropical China. *J. Meteor. Soc. Japan*, **61**, 306–312.

——, and C. C. Yu, 1988: Study of low-level jet and extremely heavy rainfall over northern Taiwan in the Meiyu season. *Mon. Wea. Rev.*, **116**, 884–891.

——, C. C. Wang, and D. T. W. Lin, 2005: Characteristics of low-level jets over northern Taiwan in Meiyu

season and their relationship to heavy rain events. *Mon. Wea. Rev.*, **133**, 20–43.

——, ——, and L. F. Lin, 2006: A diagnostic study of a retreating Meiyu front and the accompanying low-level jet formation and intensification. *Mon. Wea. Rev.*, **134**, 874–896.

Chen, Q. S., 1982: The instability of the gravity-inertia wave and its relation to low-level jet and heavy rain. *J. Meteor. Soc. Japan*, **60**, 1041–1057.

Chen, S. J., Y. H. Kuo, W. Wang, et al., 1998: A modeling case study of heavy rainstorms along the Meiyu front. *Mon. Wea. Rev.*, **126**, 2330–2351.

——, W. Wang, K. H. Lau, et al., 2000: Mesoscale convective systems along the Meiyu front in a numerical model. *Meteor. Atmos. Phys.*, **75**, 149–160.

Chou, L. C., C. P. Chang, and R. T. Williams, 1990: A numerical simulation of the Meiyu front and the associated low level jet. *Mon. Wea. Rev.*, **118**, 1408–1428.

Cuxart, J., 2008: Nocturnal basin low-level jets: An integrated study. *Acta Geophysica*, **56**, 100–113.

Ding, Y. H., 1992: Summer monsoon rainfalls in China. *J. Meteor. Soc. Japan*, **70**, 373–396.

Eliassen, A., 1962: On the vertical circulation in frontal zones. *Geofys. Publ.*, **24**, 147–160.

Fu, G., H. Niino, R. Kimura, et al., 2004: Multiple polar mesocyclones over the Japan Sea on 11 February 1997. *Mon. Wea. Rev.*, **132**, 793–814.

Hamming, R. W., 1989: *Digital Filters*. 3rd Edition. Englewood Cliffs, New Jersey, Prentice-Hall, 284 pp.

Hu Bowei, Cui Chunguang, and Fang Chunhua, 2001: Causes of a two-day successively extremely heavy rain along the Changjiang valley in the eastern Hubei Province during 21–22 July 1998. *Chinese J. Atmos. Sci.*, **25**(4), 479–491. (in Chinese)

Jiang Yongqiang, Zhang Weihuan, Zhou Zugang, et al., 2002: Mesoscale rainstorm model MRM1 and its impact test. *Journal of PLA University of Science and Technology (Natural Science Edition)*, **3**(1), 1–7. (in Chinese)

——, Wang Cangyu, Zhang Weihuan, et al., 2004: Numerical simulation of extremely heavy rain and meso-$\beta$ scale low vortex in inverted typhoon trough. *Acta Meteor. Sinica.* **18**(2), 195–210.

—— and Song Jinjie, 2010: Sensitivity experiments of a severe storm in Jiangxi Province. *Journal of Nanjing University (Natural Sciences)*, **46**(3), 261–276. (in Chinese)

—— and Wang Yuan, 2010: Effects of terrain on saddle pattern during the course of "98.7" extremely heavy rainstorm in the east of Hubei Province. *Plateau Meteor.*, **29**(2), 298–308. (in Chinese)

Long Xiao, Chen Linsheng, and Wen Lijuan, 2006: A numerical study of the structure and evolution of meso-$\beta$ scale system during the "02.6" Meiyu rainfall. *Chinese J. Atmos. Sci.*, **30**(2), 327–340. (in Chinese)

Lynch, P., and X. Y. Huang, 1992: Initialization of the HIRLAM model using a digital filter. *Mon. Wea. Rev.*, **120**, 1019–1034.

Maddox, R. A., C. F. Chappell, and L. R. Hoxit, 1979: Synoptic and mesoscale aspects of flash flood events. *Bull. Amer. Meteor. Soc.*, **60**, 115–123.

Matsumoto, S., 1973: Lower tropospheric wind speed and precipitation activity. *J. Meteor. Soc. Japan*, **51**, 101–107.

Muñoz, E., J. B. Antonio, S. Nigam, et al., 2008: Winter and summer structure of the Caribbean low-level jet. *J. Climate*, **21**, 1260–1276.

Ninomiya, K., and T. Akiyama, 1974: Band structure of mesoscale echo clusters associated with low-level jet stream. *J. Meteor. Soc. Japan*, **52**, 300–313.

Parish, T. R., 2010: Forcing of the summertime low-level jet along the California coast. *J. Appl. Meteor.*, **39**, 2421–2433.

Petterssen, S., 1936: Contribution to the theory of frontogenesis. *Geofys. Publ.*, **11**, 1–27.

Sawyer, J. S., 1956: The vertical circulation at meteorological fronts and its relation to frontogenesis. *Proc. Roy. Soc. London*, **A234**, 346–362.

Shapiro, A., and E. Fedorovich, 2009: Nocturnal low-level jet over a shallow slope. *Acta Geophysica*, **57**, 950–980.

Sun Shuqing and Zhai Guoqing, 1980: On the instability of the low level jet and its trigger function for the occurrence of heavy rain-storms. *Chinese J. Atmos. Sci.*, **4**(4), 327–337. (in Chinese)

Tao Shiyan, 1980: *The Torrential Rain in China*. Science Press, Beijing, 225 pp. (in Chinese)

——, Ni Yunqi, Zhao Sixiong, et al., 2001: *Study on the Formative Mechanism and the Forecast of the Heavy Rainfall in Summer 1998 in China*. China Meteorological Press, Beijing, 184 pp. (in Chinese)

Wallace, J. M., S. Tibaldi, and A. J. Simmons, 1983: Reduction of systematic forecast errors in ECMWF model through the introduction of an envelope orography. *Quart. J. Roy. Meteor. Soc.*, **109**, 638–717.

Whyte, F. S., M. A. Taylor, T. S. Stephenson, et al., 2008: Features of the Caribbean low level jet. *Int. J. Climatol.*, **28**, 119–128.

Xu Xiaofeng and Sun Zhaobo, 2003: Dynamic study on influence of gravity wave induced by unbalanced flow on Meiyu front heavy rain. *Acta Meteor. Sinica*, **61**(6), 655–660. (in Chinese)

Xu Yamei and Gao Kun, 2002: Simulation and analysis of meso-$\beta$ vortex over middle reaches of the Yangtze River on 22 July 1998. *Acta Meteor. Sinica*, **60**(1), 85–95. (in Chinese)

Yu Rucong, Zeng Qingcun, Peng Guikang, et al., 1994: Research on "Ya-An-Tian-Lou". Part II: Numerical trial forecasting. *Sci. Atmos. Sinica*, **18**(5), 535–551. (in Chinese)

Zeng Qingcun and Zhang Xuehong, 1981: A temporal-spatial difference scheme with complete energy conservation for compressible fluid and a harmonious splitting method. *Scientia Sinica*, **11**, 1355–1366. (in Chinese)

Zhai Guoqing, Wang Zhi, and He Bing, 2003: Formation and evolution analysis of the mesoscale vortex group in the middle and lower reaches during Meiyu of the Yangtze River. *Acta Meteor. Sinica*, **61**(6), 661–672. (in Chinese)

Zhang, D. L., and R. A. Anthes, 1982: A high-resolution model of planetary boundary layer-sensitivity tests and comparisons with SESAME-79 data. *J. Appl. Meteor.*, **21**, 1594–1609.

——, and J. M. Fritsch, 1988: A numerical investigation of a convectively generated, inertially stable, extra-tropical warm-core mesovortex over land. Part I: Structure and evolution. *Mon. Wea. Rev.*, **116**, 2660–2687.

Zhang Xiaoling, Tao Shiyan, and Zhang Shunli, 2004: Three types of heavy rainstorms associated with the Meiyu front. *Chinese J. Atmos. Sci.*, **28**(2), 187–205. (in Chinese)